

# High Performance Evaluation of Helmholtz Potentials using the Multi-Level Fast Multipole Algorithm

MICHAEL P. LINGG, Michigan State University, USA

STEPHEN M. HUGHEY, Michigan State University, USA

HASAN METIN AKTULGA, Michigan State University, USA

BALASUBRAMANIAM SHANKER, Michigan State University, USA

Evaluation of pair potentials is critical in a number of areas of physics. The classical  $N$ -body problem has its root in evaluating the Laplace potential, and has spawned tree-algorithms, the fast multipole method (FMM), as well as kernel independent approaches. Over the years, FMM for Laplace potential has had a profound impact on a number of disciplines as it has been possible to develop highly scalable parallel algorithm for these potential evaluators. This is in stark contrast to parallel algorithms for the Helmholtz (oscillatory) potentials. The principal bottleneck to scalable parallelism are operations necessary to traverse up, across and down the tree, affecting both computation and communication. In this paper, we describe techniques to overcome bottlenecks and achieve high performance evaluation of the Helmholtz potential for a wide spectrum of geometries. We demonstrate that the resulting implementation has a load balancing effect that significantly reduces the time-to-solution and enhances the scale of problems that can be treated using full wave physics.

## ACM Reference Format:

Michael P. Lingg, Stephen M. Hughey, Hasan Metin Aktulga, and Balasubramaniam Shanker. 2020. High Performance Evaluation of Helmholtz Potentials using the Multi-Level Fast Multipole Algorithm. 1, 1 (July 2020), 24 pages. <https://doi.org/10.1145/nnnnnnn.nnnnnnn>

## 1 INTRODUCTION

Physics described by hyperbolic partial differential equations (PDEs) form the backbone of a wide array of modern technologies. Solutions to PDEs governing electromagnetics and acoustics have enabled technologies that have had, and will continue to have, a broad and profound effect on our daily lives. The common thread for the wide range of phenomena described by the Helmholtz equation is understanding and manipulation of wave physics at multiple length scales. This task is increasingly challenging given the increase in geometric complexity (smaller and more complex features) and wider range of operating frequencies (requiring more precision and detail to achieve optimal performance at all frequency bands). Advances in these technologies, and engineering sophisticated yet robust systems, are intimately tied to a detailed understanding of the underlying wave physics. Today, more often than not, such insight requires simulations via high-fidelity computational tools.

---

Authors' addresses: Michael P. Lingg, Michigan State University, Computer Science and Engineering, 428 S. Shaw Ln., East Lansing, MI, 48824, USA, [linggmic@msu.edu](mailto:linggmic@msu.edu); Stephen M. Hughey, Michigan State University, Electrical and Computer Engineering, 428 S. Shaw Ln., East Lansing, MI, 48824, USA, [hugheyst@msu.edu](mailto:hugheyst@msu.edu); Hasan Metin Aktulga, Michigan State University, Computer Science and Engineering, 428 S. Shaw Ln., East Lansing, MI, 48824, USA, [hma@cse.msu.edu](mailto:hma@cse.msu.edu); Balasubramaniam Shanker, Michigan State University, Electrical and Computer Engineering, 428 S. Shaw Ln., East Lansing, MI, 48824, USA, [bshanker@msu.edu](mailto:bshanker@msu.edu).

---

Permission to make digital or hard copies of all or part of this work for personal or classroom use is granted without fee provided that copies are not made or distributed for profit or commercial advantage and that copies bear this notice and the full citation on the first page. Copyrights for components of this work owned by others than ACM must be honored. Abstracting with credit is permitted. To copy otherwise, or republish, to post on servers or to redistribute to lists, requires prior specific permission and/or a fee. Request permissions from [permissions@acm.org](mailto:permissions@acm.org).

© 2020 Association for Computing Machinery.

XXXX-XXXX/2020/7-ART \$15.00

<https://doi.org/10.1145/nnnnnnn.nnnnnnn>

One of the main challenges in developing such tools is computing fields on electrically large objects. Here, electrical length is measured in terms of the largest linear dimension in terms of wavelengths. For several emerging problems, the electrical length can be several thousand wavelengths. Creating a full-wave physics based model for such “large” Helmholtz systems represents a major challenge because at its core, a Helmholtz integral equation based solver relies on an iterative sparse solver for which the single most expensive kernel is evaluation of the potential for the corresponding  $N$ -body problem. The Fast Multipole Method for Helmholtz equations (H-FMM) reduces the  $O(N_s^2)$  cost of direct potential evaluation to  $O(N_s \log N_s)$  [9] for surface distributions. Here,  $N_s$  denotes the number of degrees of freedom. This algorithm bears a strong similarity to that developed for Laplace equations (L-FMM), i.e., for non-oscillatory potentials such as gravitational or electrostatic fields [17]. The literature on the intricacies of both L-FMM and H-FMM (and their close cousins, tree-codes) are extensive; see [3, 4, 15, 28, 32, 38]. As is evident from these review papers, applications of these algorithms is extensive and cross-cutting in terms of the number of disciplines that it has benefited.

Given the wide applicability of FMM, a number of parallel algorithms and parallel implementations have been developed. Those developed for L-FMM have indeed been highly successful in terms of their performance and scalability. Indeed, several Gordon-Bell awards have gone to scalable L-FMM algorithms [18, 21, 29, 44]. This is in contrast to the development of parallel algorithms for H-FMM, despite sustained efforts [10, 23, 24, 42]. The challenges to developing efficient parallel algorithms for H-FMM arise due to (a) the varying structure and cost of the computational workflow over the underlying tree representation, and (b) accuracy requirements of the target applications. To understand these issues better, we next present the nuances of H-FMM in comparison to L-FMM, summarize the existing literature on parallel algorithms for H-FMM and contributions of this paper that overcome some of the bottlenecks.

## 2 PROBLEM STATEMENT AND BACKGROUND

Consider a collection of  $N_s$  point sources with intensity  $u_n \in \mathbb{C}$  located at points  $\mathbf{r}_n \in \mathbb{R}^3$ ,  $n = 1, \dots, N_s$ . The potential  $\Phi(\mathbf{r})$  due to these sources at some observation point  $\mathbf{r}$  is then given by

$$\Phi(\mathbf{r}) = \sum_{n=1}^{N_s} g(\mathbf{r} - \mathbf{r}_n) u_n, \quad (2.0.1)$$

Here, the Green’s function  $g(\mathbf{r})$  for the Helmholtz equation is given by

$$g(\mathbf{r}) = \frac{e^{-jk|\mathbf{r}|}}{4\pi|\mathbf{r}|}, \quad (2.0.2)$$

where  $k = 2\pi/\lambda$  denotes the wavenumber in rad/m and  $\lambda$  is the wavelength in meters. Note, the Green’s function for the Laplace potential is recovered when  $k = 0$ . Sums of the form (2.0.1) often arise in the discretization of integral equations in electromagnetics and acoustics [6], in which  $\Phi(\mathbf{r})$  must be evaluated at each source point  $\mathbf{r}_m$ ,  $m = 1, \dots, N_s$ , implying a cost of  $O(N_s^2)$ . The multilevel fast multipole algorithm (MLFMA) [8, 33], or H-FMM as referred to in this paper, allows approximating these quantities in  $O(N_s \log^2 N_s)$  for surface distributions or  $O(N_s)$  volumetric distributions to arbitrary precision.

*Fast Multipole Methods.* Both L-FMM and H-FMM follow the same algorithmic rubric. First, the computational domain is recursively subdivided into cubes (boxes) until a pre-determined box dimension or a maximum number of particles per box is reached, and each particle is mapped to the box in which it resides. The hierarchical structure resulting from this recursive subdivision

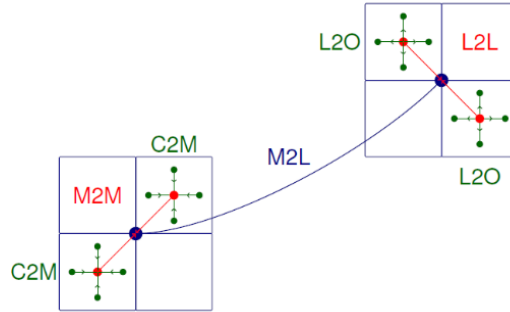


Fig. 1. Top-down view of the lowest two levels of an FMM tree, illustrating the key computational kernels. Particles (green dots) are mapped onto leaf nodes (small squares) in an octree partitioning.

procedure can be represented as a tree specifically an *octree* in which each subdivision results in the creation of (up to) eight boxes of half the diameter in 3D.

Assuming an octree with  $L$  levels, let the root node reside at level  $l = 1$ , and the leaf boxes reside at level  $l = L$ . At all levels, boxes are classified as being either in the near- or far-field of each other if they are sufficiently close. Two boxes are in each other's near-field if their domains share a face, edge or node. At any given level, two boxes are designated to be in each other's far-field if (a) they are not in the near field of each other, and (b) their parents are in each other's near-field. This permits a hierarchical partitioning of the computational domain in terms of near- and far-field interactions. Near-field calculations take place *only* at the lowest level; at all other levels, interactions between boxes is performed via far-field through a five stage process shown in Figure 1 and listed below (note, specific mathematical details are omitted in this discussion, and can be found in [16, 40] and elsewhere [28, 38]):

- (1) Compute charge to multipole information for each leaf node based on the particles it encloses (C2M),
- (2) compute the multiple expansions for each node in the tree by interpolating from the multipole information of all of its children (M2M),
- (3) calculate interactions between far-field pairs by translating multipole expansions of sources to the observers' locations (M2L),
- (4) starting at the highest level nodes and going all the way down to the leaves, distribute (interpolate) multipole expansions aggregated at non-leaf observer boxes as a result of M2L (these expansions are then referred to as *local expansions*) to their children (L2L),
- (5) convert the resulting local expansions at each leaf box to particles enclosed therein (L2O).

*Laplace vs. Helmholtz FMM and Ramifications on Parallelization.* As alluded to earlier, highly efficient parallel implementations of L-FMM exist [21, 29] in contrast to those for H-FMM [14, 20, 25, 42]. To understand why, one needs to examine the underlying mathematics.

- In L-FMM, irrespective of the tree level, the amount of multipole data needed to be stored at each node in the tree is identical because the magnitude of a Laplace potential monotonically decreases with distance.
- Due to the constant information content in L-FMM nodes, the per-level cost of far-field interactions falls off exponentially, and the bulk (80-90% or more) of the work in L-FMM is associated with the leaf nodes. Thus, existing L-FMM efforts have focused on optimizing the computation and masking communication costs primarily at the leaf level [2, 34, 43].

- In contrast, in H-FMM the amount of multipole data associated with a node depends on the level due to the oscillatory nature of the potential. More precisely, the amount of multipole data in a parent must be at least four times larger than that of its children to ensure that the desired level of accuracy can be obtained. This fundamental difference leads to major scalability and memory bottlenecks in H-FMM implementations [19, 23].
- Due to the quadrupling of the information content as one ascends an H-FMM tree, computational and memory costs in H-FMM stay constant for each tree level for surface geometries and halves for volumetric problems. For this reason, advances in parallel L-FMM do not translate readily to parallel H-FMM despite significant and sustained research [11, 13, 14, 35, 37, 39]. The commonly-used local essential tree (LET) [30] paradigm from the L-FMM literature fails for H-FMM because the size of the "ghost" region representing sources residing on other processes rapidly exceeds available memory.

Addressing these performance and scaling challenges, while maintaining high accuracies in potential evaluations, constitutes the main motivation for the present work.

*Related Work.* The aforementioned work profile of the H-FMM octree suggests that any efficient parallelization must strike a balance between distributing the many lightweight boxes at lower levels and distributing the work of the few heavyweight boxes at higher levels across processes. Furthermore, the mathematics used to effect each stage of the process dictate the intricacies of the algorithms developed for parallelization. The existing algorithms address these different scenarios with different trade-offs. For the purposes of the ensuing discussion, we note that multipole and local expansions may be viewed as two-dimensional arrays of sampled function values.

At scale, the multipole and local expansions of octree boxes at the uppermost levels of the tree must be distributed across processes to achieve load balance [36]. To reduce the costs of communication in M2M and L2L for these distributed nodes, several authors have employed *local* interpolation techniques [7, 12, 25], in which only a small "halo" of nearby samples are required to calculate each new sample. However, despite slightly reducing the H-FMM's asymptotic complexity from  $O(N_s \log^2 N_s)$  to  $O(N_s \log N_s)$  [5], this approach increases memory and computational costs stemming from the need to oversample multipole and local expansions, in addition to reducing the numerical accuracy of the H-FMM. Alternatively, we propose the use of a parallel version of the *global* interpolation method, which has typically remained restricted to the serial M2M/L2L operations at lower levels of the tree. Though the global algorithm obviously has higher communication costs, it does not introduce additional numerical errors, and it facilitates optimal (minimum) sampling rates for multipole/local expansions [20, 22].

Local interpolation based hierarchical partitioning (HiP) approach distributes expansions hierarchically at the uppermost levels in block columns, or strips [12]. However, the M2M and L2L communication costs scale as  $O(\sqrt{N_s})$  per process, hampering the scalability of the H-FMM evaluation [14]. The blockwise HiP (B-HiP) strategy [25, 27] alleviates this bottleneck by distributing expansions in blocks, whose much lower surface-to-volume ratio results in  $O(1)$  communication costs per process, hence improving scalability [26]. In both methods, M2L operations are carried out in parallel by collecting on each process samples of the remote multipole expansions required to compute the local expansions it owns. It should also be noted that the increased sampling required with local interpolations hampers the scalability of the M2L phase, as collecting remote multipole expansions requires a significantly higher communication bandwidth compared to a global scheme with optimal sampling rates.

Building on the HiP approach, Yang et al. [42] transition from hierarchical partitioning to plane-wave partitioning (PWP) [36] for the highest levels of the tree, using a binary tree decomposition of the MPI communicator to flexibly load balance the computation. The PWP approach achieves

zero communication overhead for M2L operations by distributing expansions at the uppermost levels of the tree by assigning each process a fixed window of samples for *all* expansions at a given level. However, the transition from HiP to PWP requires expensive communications in M2M and L2L phases to rearrange the expansions, though this cost may be justified by recognizing that each node interacts with at most 8 other nodes to perform the M2M/L2L operations, while the maximum number of nodes for M2L operations is 189 (with a volumetric problem).

As previously stated, local interpolation methods are convenient for parallelization but result in an H-FMM that is **not** strictly error-controllable. The principal challenge to a scalable H-FMM with error control is the communication cost of distributed global (exact) interpolation. In [23], Melapudi et al. describe an error-controllable H-FMM based on global interpolation using a bottom-up partitioning which gives great flexibility for load balanced partitioning of the tree. Scaling of this implementation is hampered by the coarse-grained parallelization of the M2L phase and redundant M2M/L2L calculations associated with high-level tree nodes shared by multiple processes.

*Contribution.* In this paper, we build upon our earlier efforts [20, 23] toward a scalable, error-controllable H-FMM based on global interpolation. We address several challenges regarding parallelization and communication, and we demonstrate an efficient and scalable method for evaluation of the Helmholtz potential. In particular, our contributions can be summarized as follows:

- (1) Development of a fine-grain parallel algorithm with bottom-up partitioning that enables scalable evaluation of deep uniform MLFMA trees,
- (2) maintain the high level of controllable accuracy shown in previous global interpolation implementations,
- (3) a detailed analytical model to characterize the complexity and memory use of the parallel algorithm for far-field interactions,
- (4) and, demonstration of the overall algorithm performance and validation of this performance against our analytical model for different test scenarios.

### 3 PARALLEL ALGORITHMS AND IMPLEMENTATIONS

In what follows, we describe details of each stage of the algorithm. For completeness, we replicate some of the concepts introduced in [20, 23], before delving into details of our specific contributions.

#### 3.1 Tree construction and setup

Let  $N_p$  denote the number of processes used in the computation. We initially distribute the  $N_s$  particles evenly across all processes and determine the diameter  $D_0$  of the cube bounding the entire computational domain. Given the finest box diameter  $D(L)$ , the number of levels in the tree is calculated as the smallest integer  $L$  such that  $L \geq \log_2(D_0/D(L)) + 1$ . Once the number of levels and therefore the position of the leaf nodes are known, every particle is assigned a key based on the Morton-Z order traversal of the MLFMA tree [41]. A parallel bucket sort on the Morton keys is then used to roughly equally distribute particles across processes at the granularity of leaves. This is done by selecting  $N_p - 1$  Morton keys, or “splitters”, which chop the Morton Z-curve into  $N_p$  contiguous segments. Whole leaves are uniquely assigned to processes using these splitters. Given a contiguous segment of leaf nodes, each process determines all ancestor keys of its leaves up to the root. The leaf through ancestor nodes are used to construct the *local subtree*. A simple method of storing the local subtree is as a post-order traversal array. To quickly access a random node, we use an indexer into this local subtree array.

*Plural Nodes.* Despite the non-overlapping partitioning of leaf nodes, overlaps among different processes at the higher level nodes are inevitable (and in fact, are desirable) as illustrated in Fig. 2.

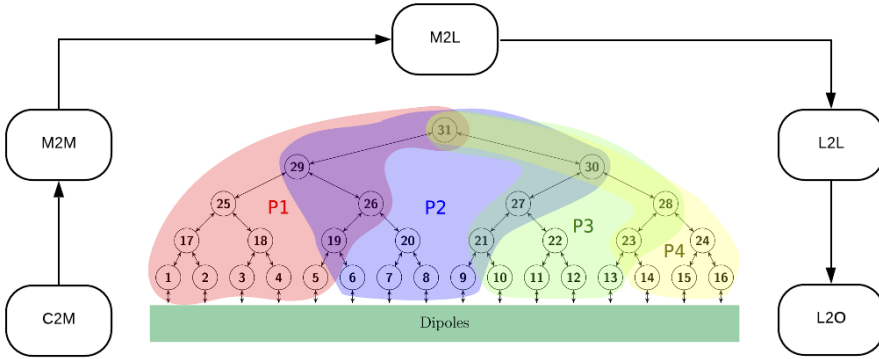


Fig. 2. Parallel Farfield MLFMA.

Details and associated proofs on such partitioning can be found in [23]. We call such nodes shared by multiple processes as *plural nodes*. While there are no limitations to the number of processes that can share a plural node, we designate a particular process, i.e., the right-most process sharing the plural node in the MLFMA tree, as its *resident process*. We refer to the resident process' copy of a plural node as a *shared node* and all other copies of this node residing on other processes as *duplicate nodes*. We call the set of processes that own these duplicate nodes as *users* of the shared node, denoted by  $U(s)$ , where  $s$  is the shared node.

One notable advantage provided by plural nodes is that storage of the node is split between multiple processes. In this case, the indexer additionally stores which *slice* of a tree node the current process actually stores in its local subtree array. As the information content for a node is not available to any single process in its entirety, a fine grain parallelization is necessary to perform computations associated with plural nodes. We note that a process can have at most two plural nodes per level in its local tree (essentially one to the “left”, and another to the “right”).

### 3.2 Parallel Evaluation

**3.2.1 C2M.** C2M is unchanged from our previous works [20, 23]. As each process is assigned a contiguous segment of whole leaf nodes, each process handles the C2M phase for its assigned leaf nodes in parallel independently.

**3.2.2 M2M.** In a nutshell, M2M creates multipole expansions of non-leaf boxes from the multipole expansions of their children. This first requires multipole expansions of all children to be *interpolated* to the size of the parent box. Next, each interpolated child box is *shifted* from the center of the child box to the center of the parent box. Finally, multipole contributions of every shifted child box are *aggregated* to form the multipole expansion for the parent box.

M2M computations start at the leaf level and proceed upwards in the tree following a post-order traversal of the local tree. Our parallelization of M2M depends on the level of the node and is described in Alg. 1. The approach is as follows: i) Non-plural tree nodes (that are typically found at lower levels of the tree) are handled by their owner processes in parallel independently, ii) for plural nodes without any plural children, *interpolation* and *shift* steps for child nodes are performed sequentially, and the aggregation step is performed as a reduce-scatter operation among processes sharing the plural node, iii) plural nodes with plural children (which typically are located at the

higher levels of the tree and incur significant computational and storage costs) are processed using a fine-grained parallel algorithm that we discuss in more detail below.

---

**Algorithm 1** Multipole-to-multipole interpolation
 

---

**Require:**  $p.center$  coordinates of the parent box center

**Ensure:**  $pmp$  is parent's multipole representation

```

1: for each box  $p$  in post-order traversal do
2:   for each child box  $c$  do
3:     if  $c$  is plural then
4:        $mp[c] \leftarrow \text{parallel\_interpolation}(c)$ 
5:     else
6:        $mp[c] \leftarrow \text{serial\_interpolation}(c)$ 
7:     end if
8:      $smp[c] \leftarrow \text{shift}(mp, p.center)$ 
9:   end for
10:  if  $p$  is plural then
11:     $\text{reduce\_scatter}(smp, users(p))$ 
12:  else
13:    for each child box  $c$  do
14:       $\text{aggregate}(pmp, smp[c])$ 
15:    end for
16:  end if
17: end for

```

---

*Fine-grained Parallel Interpolation.* For plural nodes that necessitate fine-grained parallelization of M2M, the multipole data of the child nodes needed for FFTs are themselves split among multiple processes as indicated in Alg. 1. Prior to elucidating our parallel algorithm, we note that our M2M implementation uses a Fast Fourier Transform (FFT)-based interpolation over the uniformly spaced multipole expansions of the child nodes [31]. FFT-based interpolation on the Fourier sphere requires equispaced samples along  $\theta$  (vertical) and  $\phi$  (horizontal) directions. Due to the inter-dependencies of the FFT algorithm, there is no way to partition the data so as to avoid communication.

Our approach is as follows: First, each process is assigned a (roughly) equal number of contiguous columns of multipole data (which correspond to groups of samples along the  $\phi$  direction). The operation begins with a set of independent FFTs along these columns for interpolation in the  $\phi$  direction, performed the same as the basic Sarvas approach. Then, the interpolated columns are shifted into rows (see Fig. 3), transposing and folding the samples in the  $\theta$  direction into individual columns. The next step with serial processing would be FFT interpolation in the  $\theta$  direction, but this data is split between processes sharing the plural node. Therefore, each process is communicated the  $\theta$  samples they need to complete their assigned columns using an `MPI_Alltoallv` collective call. Now that each process is storing full columns of  $\theta$  samples, these multipole data can be interpolated. The fully-interpolated multipole data is transposed and folded back to its original form ( $\phi$  samples along columns,  $\theta$  samples along rows). The data are again communicated back to the processes that own the corresponding multipole samples via another `MPI_Alltoallv`. These major steps are illustrated in Figure 3.

*Shifting of Interpolated Data.* Shifting of multipole data is simply the translation of the interpolated samples from the child node's center to the parent node's center. Translation of each multipole data is independent of others and trivially parallelizable even in the case of fine-grained parallel M2M.

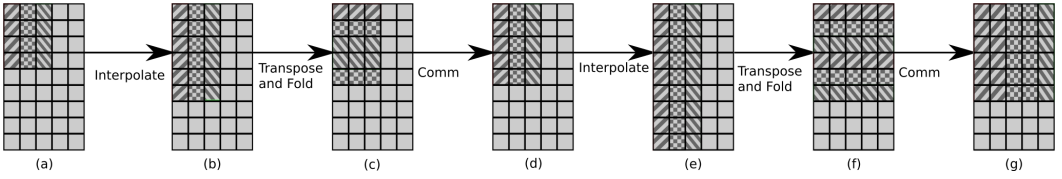


Fig. 3. Graphical illustration of the transposition and folding operations during fine grained parallel interpolation of multipole data of child node  $c$  to parent node  $p$  for  $N_\theta = 3, N_\phi = 4$  (for  $c$ ) and  $M_\theta = 5, M_\phi = 6$  (for  $p$ ) using 3 processes each of which owns a column of the initial multipole data as indicated by the hashmarks. Multipole data from (a) is interpolated along the  $\phi$  dimension locally, leading to the multipole expansions in (b). The folding operation acting on the interpolated data is shown by the repositioning of the data as in (c). The hash marks show how the folded data is stored on the wrong processes, and must be communicated to the correct process as shown in (d). With the entire multipole data columns in the  $\theta$  direction being available on each process, another set of interpolations are performed locally (e), which is then transposed and folded to yield the final multipole expansions (f). A final communication step is needed to send each  $\theta$  vector to their own processes (g) which can then be shifted to the center of the parent box and added to the parent's multipole expansions in accordance with the spherical symmetry condition.

**Aggregation.** Aggregation requires adding all corresponding samples from each interpolated and shifted child node together to form the multipole expansion of a parent node (step (g) in Fig. 3). When children are owned by separate processes (as is the case for plural nodes), reduction communications are required. Note that in fine-grained parallel M2M for a plural node, each process owns only a portion of the parent node's multipole data. A reduce/scatter operation (for instance using `MPI_Reduce_scatter`) could perform both the aggregation and distribution of the appropriate portions of the aggregated multipole data to the processes sharing a plural node. One complication here is that the reduce/scatter operation would require memory to be allocated to the full-size of the parent node by each user process through padding the parts not owned by a process with 0s. Clearly, this would lead to significant memory and computational overheads, especially at the highest levels of the H-FMM tree (due to the large sizes of the plural nodes there). Therefore, we opt for a custom point-to-point aggregation scheme where the interpolated and shifted multipole samples from child nodes are communicated directly (via `MPI_Send` and `MPI_Recv`s) to the process that owns the corresponding samples of the parent node. If the source and destination are the same process, obviously no communication is performed. Each process sharing the parent node then adds up the corresponding multipole samples it receives from each child node, local or communicated. This method reduces both the amount of temporary memory necessary for aggregation and the overall communication volume.

**Process Alignment.** In fine-grained parallel M2M, performance impact of how the multipole data of child and parent plural nodes are mapped to processes sharing those nodes also needs to be considered. From the description of our custom point-to-point aggregation scheme above, it is evident that increasing the overlap of the multipole sample regions owned by a process in the child and parent nodes is critical for reducing the communication volume. As an extreme example, if a process owns no samples in the parent node that correspond with any of the samples it owns in the child node, all its interpolated and shifted child node samples would have to be communicated to another process for aggregation. In fact, this extreme example is not uncommon when multipole data of a node is simply partitioned into blocks and mapped to user processes according to their process ranks. This situation is illustrated on the left side of Fig. 4; some processes own samples of a parent node that has no overlap with the samples they own in the child node. Specifically,

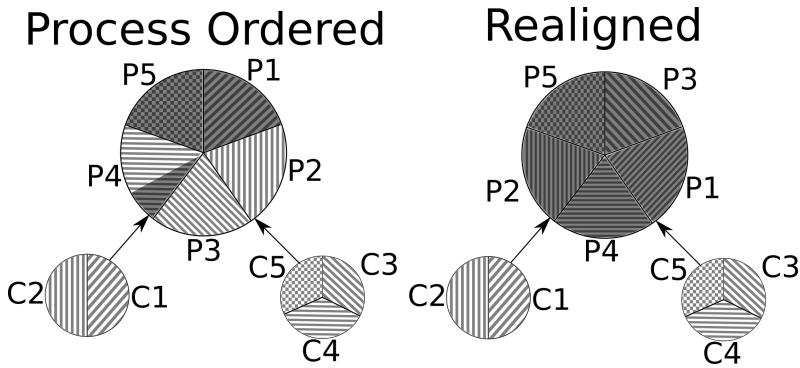


Fig. 4. This image shows how multipole samples, ordered clockwise starting at 12 o'clock, are assigned to processes owning the children nodes (C1-C5) overlap with processes owning the parent node (P1-P5) when assigned in process rank order on the left, and with our realignment scheme on the right. The darker portions on the parent samples show the regions where the parent node data overlap with the child node data, and are essentially local data that do not require communication.

while process 1 owns overlapping samples in the child and parent nodes, process 2 and 3 own no overlapping samples.

As a heuristic to minimize the communication volume, we order processes within a parent node such that the parent node samples are assigned by following the priorities below to ensure maximal overlap with their child node samples:

- (1) Index of the lowest sample they own in the child nodes (lower comes first),
- (2) number of samples they own in the child nodes (fewer comes first),
- (3) process rank.

In the example given in Fig. 4, both process 1 and process 3 own samples with index 0 in the child nodes, but process 3 has a smaller number of samples so it is assigned the first portion of the parent node samples with process 1 being assigned the second portion. Following processes 3 and 1, process 4 owns the multipole sample with the lowest index in the child nodes, followed by process 2, and then process 5. As such, remaining portions of the parent node samples are assigned in this order. As can be seen in the figure, all samples each process owns in the parent node fully overlap with samples that they own in the child nodes, despite the non-uniform layout. With the proposed process alignment scheme, process 3 will still need to communicate some samples to process 1 for aggregation, but over half of the child samples interpolated by process 3 remains local. Note that with the straight-forward ordering of processes by their ranks, the entire child data interpolated by process 3 would have to be communicated to processes 1 and 2. In the new scheme, all processes use interpolated samples from their part of a child node without having to communicate. While this scheme would work best with a perfectly balanced tree, this approach will still be effective in reducing the communication volume during aggregation with any tree structure.

**3.2.3 M2L.** The M2M step builds the multipole expansions of all tree nodes owned/shared by a process, starting from the leaves all the way up to the root (or the highest level of computation). During M2L each observer node loops through all source nodes in its far-field and translates the source multipole data to its locale, aggregating the effects from all its far-field interactions in the process. When the source-observer node pair is on the same process, this interaction is handled purely locally. However, when the source node data is on another process (or a set of processes), one needs a load balanced algorithm that is communication efficient.

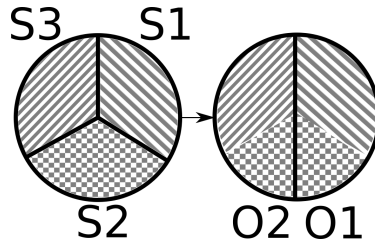


Fig. 5. A translation operation between two plural nodes shared by different numbers of processes.

To understand the scope of the problem, consider Figure 5. Here, the source node is a plural node shared by three processes (S1, S2 and S3); the observer node is shared by two processes (O1 and O2). Multipole samples for both are shared starting at the top of each circle and increasing clockwise (consistent with the process alignment scheme utilized during M2M). Process S1 and O1 both own multipole samples with the lowest indices, with S1 having less samples than O1. For this far-field interaction, S1 would need to send all samples that it owns to O1. S3 and O2 both own samples with the highest indices; here S3 would need to send all of its samples to O2. Finally, S2 owns samples that are needed by both O1 and O2, therefore S2 must send half of its samples to O1 and the other half to O2. Since each node in the H-FMM tree interacts with several others ( $\approx 27$  for surfaces and up to 189 for volumes) each of which may be shared by a varying number of different processes, it is evident that coordination of all communications that must take place during an H-FMM evaluation is non-trivial.

In an initialization step before the actual M2L operations, all processes discover the owner process(es) of the tree nodes (i.e., observers) which will need the multipole data for the source nodes they own, given the partitioning of leaf nodes (for load balancing purposes) and process alignments for plural nodes. This pre-calculated list is formed to carry out the actual communications that will take place during the ensuing H-FMM potential evaluations. If a source node or the corresponding observer node is plural, then the pre-calculated communication list will include only the intersection of the multipole data owned by both the source and target processes. When a source node on a process is needed by multiple observers on another process, it is sufficient to include the source node in the communication list to that other process only once. Also, multipole data for multiple source nodes residing on one process that are needed by another can be combined into a single message in this communication list, even if the source nodes are at different levels. Note that the tree structure in most H-FMM applications are fixed. As such, the overheads associated with such an initialization stage is minimal.

While plural node to plural node far field interactions (which constitute the most expensive communications in an H-FMM evaluation) could actually be carried out using all-to-all communications that involve only the users of the two corresponding plural nodes, due to the excessive number of M2L interactions present in large-scale computations (and hence the large number of different communicators that must be created), we choose to perform these communications using non-blocking point-to-point send/rcv operations (i.e., MPI-Sends and MPI-Ircvs) in the default global communicator. Another reason for opting for a point-to-point scheme is that there are significant differences in the amount of data that must be sent to one process compared to another. As part of the initialization step then, each process allocates a message buffer for every other process that it will communicate with. The size of the send buffer is limited to avoid excessive memory use and maximize communication overlap.

**Algorithm 2** M2L Translation

---

```

1: Determine the union of data owned by both source and target.
2: procedure M2L
3:   for each source box do
4:     for each farfield interaction target do
5:       if Target box is not local then
6:         for each process sharing target box do
7:           Add source multipole data in union of data owned by both source and target
           to buffer.
8:         end for
9:       end if
10:    end for
11:   end for
12:   Communicate buffers between processes.
13:   for each target box do
14:     for each farfield interaction source do
15:       if Source box is local then
16:         Load source multipole data from local memory.
17:         Translate source multipole data to target and add to existing translated data for
           target node
18:       else
19:         for each process sharing source box do
20:           Read source multipole data from communication.
21:           Translate source multipole data to target and add to existing translated data
           for target node
22:         end for
23:       end if
24:     end for
25:   end for
26: end procedure

```

---

To perform communications during M2L, every process first fills their send buffers for each process based on the pre-calculated communication list and initiates the message transmission using `MPI_Isends`. Immediately after initiating the sends, each process starts waiting for their expected messages using `MPI_Irecvs`. The status of these communications are checked periodically. Computations are overlapped with M2L communications in two ways. First, blocks of translations that are entirely local (which is actually common at the lower tree levels) are processed while the non-blocking send/recvs are taking place. Second, translation data that is detected as received during the periodic checks are applied immediately, overlapping the corresponding computational task with communications underway. Due to the limit we impose on the message buffer sizes, communications with processes that involve a large amount of data transfer need to be performed in multiple phases. Hence, upon reception/delivery of a message from another process, if there is more data to be transferred, a new non-blocking recv/send operation is initiated.

*Translation Operators.* Source node data is translated to the target node by multiplying it with a translation operator. The translation operators can be pre-calculated to reduce computational costs. As these can potentially take significant memory, we limit such memory use by each process by

having them store the pre-calculated operators only for translation of the local and remote samples that they will actually need. This information can be determined from the pre-calculated M2L communication list. In case the memory available is not sufficient to store the needed operators, we use techniques outlined in [20] to sample and interpolate translation operators.

**3.2.4 L2L.** To antepolate and distribute the translated local expansions down to the child nodes, L2L applies the operations in M2M in reverse order. First, local expansions at the parent node are shifted to the center of each child node, they are then antepolated and percolated down the tree. Finally, the antepolated data is aggregated with local expansions previously translated to the child node during the M2L stage.

Much like M2M, L2L operation is parallelized in three different ways: i) Non-plural parent tree nodes at the lower tree levels are processed independently in parallel by their owner processes, ii) for a plural node with a non-plural child, shifts involve communications, but the ensuing antepolation and aggregation (with translated local expansions) are performed sequentially by the process owning the child node, iii) plural nodes with plural children require fine-grained parallelization.

*Shift.* In a parallel shift operation, parent node samples corresponding to those of the child node must be communicated by the processes sharing the parent node to the process(es) owning the child node. This is most easily done before the data has been shifted, as the parent will not need to know the position of the child node. In case of plural parent and non-plural child, this communication would essentially be a *gather*, and in case of plural parent with a plural child, it would be an *all-to-all*, in both cases involving all processes sharing the parent node. However, only a subset of the processes sharing the parent node will actually share the child node. To avoid non-trivial issues that would arise from having to coordinate several collective calls among different subsets of processes, we again resort to point-to-point communications instead. Consequently, messages are only sent from processes owning a piece of the parent node to a process owning the corresponding piece of the child node. Once a process gathers all of necessary samples of the parent node, it applies the shift operation to all its multipole samples independently.

*Antepolation.* Antepolation would have to be performed in parallel only if the child node is a plural node. The procedure for parallel antepolation is exactly the same as that of the parallel interpolation, except that the number of multipole samples is reduced (rather than increased).

*Aggregation.* Aggregating the shifted and antepolated parent data with translated local expansions is trivial. Even in the case of plural child nodes, all required data is already available locally.

**3.2.5 L2O.** As in C2M, each process handles the L2O computations of its assigned leaf nodes in parallel independently.

## 4 COMPUTATIONAL AND COMMUNICATION COMPLEXITY ANALYSIS

In this section, we analyze the asymptotic computational and communication complexity of the parallel H-FMM algorithm described above. To simplify the analysis, we focus on two extreme cases, a 2D surface represented by points on a regularly spaced planar grid (dimension  $d=2$ ) and a 3D volumetric structure represented by points on a regularly spaced cubic grid ( $d = 3$ ). These represent extreme cases, and hence are ideal for asymptotic analysis.

Let  $K(l)$  denote the number of samples in the  $\theta$  and  $\phi$  directions for a node at level  $l$ . Assume that each leaf node contains  $\mathcal{O}(1)$  samples. It follows that the number of leaf nodes is  $\propto N_s$ , the number of source points. For simplicity and with no loss in generality, we assume that the constant of proportionality is 1. Next, we denote the number of nodes at level  $l$  by  $G(l)$ . The total number of

levels is given by  $N_L$ . As one moves up the octree, we observe that the number of groups per level is reduced by roughly 4 times for the 2D surface and 8 times for the 3D volume. Leveraging the relation between the dimensionality of a structure and the rate of decrease in the number of nodes per level, one can write  $G(l)$  as follows:

$$G(l) = \frac{N_s}{(2^d)^{(l-1)}}. \quad (4.0.1)$$

Since  $K(l)$  doubles at each level, given  $K(1) = C_k$ , it follows that

$$K(l) = 2^{(l-1)}C_k. \quad (4.0.2)$$

Finally, we define  $P$  as the number of processes,  $P_L$  as the level where (almost) all nodes in a level start becoming plural and  $P_N(l)$  as the average number of processes sharing a plural node at level  $l$ . Equivalently,  $P_L$  is the level when  $G(P_L) < P$  for the first time, and this remains true from hereon to the root. Given  $P$ ,  $N_s$  and  $d$ ,

$$P_N(l) = \frac{P}{G(l)} = \frac{P(2^d)^{(l-1)}}{N_s} \quad (4.0.3)$$

#### 4.1 Interpolation (M2M)

*Computational Complexity.* M2M is performed for each node, starting from the leaf level up to the highest level  $N_L$ . The dominant component in the computational complexity for M2M is FFT-based interpolation. Shifting and aggregation are  $O(K(l)^2)$  operations each, while interpolation for a given node costs  $O(K(l)^2 \log^2(K(l)))$ . This gives a total computational complexity of

$$C \propto \sum_{l=1}^{N_L} G(l)K(l)^2 \log^2(K(l)) \quad (4.0.4)$$

Plugging in the equations (4.0.1) and (4.0.2) and simplifying the summation, we obtain the computational complexity for a surface to be:

$$C \propto O(N_s \log^2 N_s), \quad (4.0.5)$$

and for a volume to be:

$$C \propto O(N_s) \quad (4.0.6)$$

*Number of Messages (Latency).* Communication in M2M happens during aggregations for both coarse-grained and fine-grained parallel M2Ms, as well as the FFTs of the fine-grained parallel M2Ms. As described in Sect. 3.2.5, we perform aggregations (which are effectively reduce-scatter operations) using point-to-point communications. In an ideal tree, every source and observer node will be divided among the same number of nodes. This means the portion of a source node owned by any process will only be owned by a single process in the observer node, limiting the communication for each source node process to one process in each observer node. Since this is done for each group at each level, the total message count for aggregations can be written as:

$$M_{Ag} \propto \sum_{P_L}^{N_L} G(l)P_N(l+1). \quad (4.0.7)$$

Using expressions for  $P_N(l+1)$  and  $G(l)$ , yields the number of messages for aggregation

$$M_{Ag} = O(P \log(N_s) 2^d). \quad (4.0.8)$$

Here, we ignore aggregations that would be needed for plural nodes (located at process boundaries) below level  $P_L$ . Note that there may only be two such plural nodes per level for each process and these aggregations will involve only two processes. As such, their contribution to the number of messages during aggregations is of a lower order term.

Next, consider the parallel FFTs in fine-grained parallel  $M2Ms$ . In this case, an all-to-all communication is performed after each of the two fold and transpose operations. As we implement these all-to-all communications using point-to-point calls, the message count for FFTs is then:

$$M_{FFT} = \sum_{l=P_L}^{N_L} G(l)P_N(l)^2 \propto O(P^2). \quad (4.0.9)$$

Consequently, the total number of messages for  $M2M$  is:

$$M_{M2M} = O(P^2 + P \log(N_s)). \quad (4.0.10)$$

Note, the  $N_s$  portion of the equation above is only going to matter when  $P_L$  is greater than the number of levels in the tree. In all other cases, increasing the height of the tree does not increase the number of levels with plural nodes. Given that it is practically useless to have more processes than the number of leaf nodes (which is the condition required for  $P_L$  to be more than the tree height), the message count can be simplified to  $M_{M2M} = O(P^2)$ .

*Communication Volume (Bandwidth).* Bandwidth during interpolation is due to all to all communications during interpolation, and a reduce scatter during the aggregation. Each of these operation communicates up to the entire node, resulting in a bandwidth that can be written as:

$$B \propto \sum_{l=1}^{N_L} G(l)K(l)^2 \quad (4.0.11)$$

Applying the previous definitions for  $G(l)$  and  $K(l)$  yields a communication bandwidth of  $B \propto N_s \log N_s$  for the surface geometry, and  $B \propto N_s$  for the volume geometry.

## 4.2 Translation (M2L)

*Computational Complexity.* The complexity for the translation operation at a given level is directly proportional to the number of multipole samples for nodes, the average number of interactions per node (denoted by  $I(l)$  for level  $l$ ), and the number of nodes at that level. Summing these costs across all levels, we obtain:

$$C \propto \sum_{l=1}^{N_L} K(l)^2 I(l) G(l). \quad (4.0.12)$$

While the number of interactions for a node changes based on its exact position in the geometry (for instance, corner or edge nodes), the upper limit is the constant  $6^d - 3^d$ . Using the equations for  $K(l)$  and  $G(l)$ , computational complexity of the translation step can be simplified to  $O(N_s \log N_s)$  for the surface structure, and to  $O(N_s)$  for the volume structure.

*Number of Messages (Latency).* At level  $P_L$  or above, a process can have multipole samples for only one node. Since a process owns at most part of a single node, each of its interactions will require a separate communication because the nodes in its far-field will all reside on different processes. Assuming an ideal tree partitioning where the source and target nodes are shared among the same number of processes, the  $k$ th process for the target node will only need the source node data from the  $k$ th process of the source node. As we limit the size of each translation message, the number of messages will then be proportional to the communication volume between a pair of

processes divided by the message buffer size  $M_S$ . At levels below  $P_L$ , a process can own multiple nodes. Here groups of nodes can be communicated to the same process, if all source nodes reside on one process and all observer nodes reside on another. In this case, the interaction count is going to be based on the total amount of data communicated between the two interacting processes, divided by the message buffer size, summed up for all interacting processes.

Considering contributions at/above  $P_L$  and below  $P_L$  gives a total message count of:

$$M \propto \sum_{l=P_L}^{N_L} PI(l) \frac{K(l)^2}{P_N M_S} + PI(l) \left[ \frac{\sum_{l=1}^{P_L-1} K(l)^2 \frac{G(l)}{P}}{M_S} \right] \quad (4.0.13)$$

where  $M_S$  is the size of message buffers. For the surface geometry, this can be simplified to  $M \propto O(N_s \log N_s) + O(N_s)$  (where the first term is for levels  $\geq P_L$  and the second term is for levels  $< P_L$ ), and for the volume geometry it can be simplified to  $M \propto O(N_s)$  (with both below and above  $P_L$  having the same impact).

*Communication Volume (Bandwidth).* Similarly, communication volume can be analyzed in two parts as well. At and above  $P_L$ , all multipole data for every source node must essentially be communicated to every target node as no process contains any multipole data other than its own. Even if the number of processes increases, still the same amount of data needs to be transmitted, just among an increased number of nodes. Therefore, for level at or above  $P_L$ , the communication volume is independent of the number of processes:

$$B \propto \sum_{l=P_L}^{N_L} K(l)^2 G(l) I(l) \quad (4.0.14)$$

This expression simplifies to  $O(N_s \log N_s)$  for the surface geometry and to  $O(N_s)$  for the volume geometry.

Below  $P_L$ , each process will own more than one node, nodes will be interacting with nodes on the same process, or multiple nodes owned by a neighboring process. In fact, only nodes within two nodes off the edge of process boundaries will require communications with other processes. Total communication bandwidth can then be expressed as:

$$B \propto \sum_{l=1}^{P_L-1} PK(l)^2 (S_N) \quad (4.0.15)$$

where  $S_N$  is the number of nodes that have nodes in its far-field from at least one (out of the 8 possible neighboring processes for the surface and 26 for the volume) other processes touching them and can be represented as  $S_N = \frac{G(l)}{P} \frac{d-1}{d} = \frac{1}{P} \left( \frac{N_s}{(2^d)^{(l-1)}} \right) \frac{d-1}{d}$ . With this definition of  $S_N$ , the total communication volume for M2L below  $P_L$  becomes

$$B \propto O(N_s) \quad (4.0.16)$$

for the surface, and

$$B \propto O(N_s^{\frac{2}{3}}) \quad (4.0.17)$$

for the volume, due to the lower portion of the tree dominating.

### 4.3 Anterpolation (L2L)

As mentioned before, L2L is the reverse operation for M2M. Similar to M2M, anterpolation dominates the computational complexity for L2L. Computational complexity for anterpolations is the same as that of interpolations, so L2L's computation complexity is the same as M2M's. Likewise,

communications performed are the same but in reverse order. Therefore, the latency and bandwidth costs of L2L are the same as those of M2M.

## 5 PERFORMANCE EVALUATION

In this section, we evaluate the performance of the parallel H-FMM algorithm described. All results were obtained on the Cori-Haswell supercomputer at National Energy Research Scientific Computing Center (NERSC). Each node on this system contains two sockets, populated by Intel Xeon E5-2698 v3 (Haswell) processors with a clock speed of 2.3 GHz. Each node has 32 cores and 128 GB 2133MHz DDR4 RAM. The code is implemented in Fortran 90 using only MPI parallelization and was compiled with the Intel compiler. The FFTW library is used for all FFT operations.

The runs here focus on the timing of the M2M, M2L and L2L phases of the tree traversal. As such, each leaf node is only populated with a single unknown, effectively bypassing the near-field, C2M and L2O processing steps. This also makes the number of unknowns being processed much smaller than what could be processed by M2M, M2L and L2L in the same amount of time. In a typical  $0.25\lambda$  leaf box (as we use in the runs below) with a  $0.1\lambda$  discretization rate, the number of Rao-Wilton-Glisson (RWG) functions will be around 20-30. The number of particles per box to simulate 20-30 RWG functions can range from 100-180 particle to box. Our largest tree being processed is 14 levels with 42 million points for one point per leaf box. If the leaf nodes were fully populated, this tree would be equivalent to processing a tree with 4.2 to 7.5 billion points. Populating leaf nodes would increase the time of the C2M and L2O steps, but have no impact on the execution times of the M2M, M2L and L2L phases.

### 5.1 Load balance with the fine grain parallel algorithm

The intent of the fine-grain parallel algorithm is to provide improved balance at the upper levels of the tree where a lower number of much larger nodes reside. First, we look at the performance of a planar grid of particles (in the  $z = 0$  plane) of dimensions  $512\lambda \times 512\lambda$  with a grid spacing of  $\lambda/4$  and 4,194,304 particles in total. The box size is chosen to be  $0.25\lambda$ , resulting in a 12-level tree with 10 levels of computation. As can be seen in the left subfigure of Fig. 7, the resulting execution profile is very balanced across process ranks. Execution time of the fastest to the slowest process varies by only 1.43%. Balance of total time can be a little misleading as M2L cannot progress until all processes that a given process interacts with have completed their M2M processing. However, the M2M execution times are also very balanced, varying from slowest to fastest process by 5.23%.

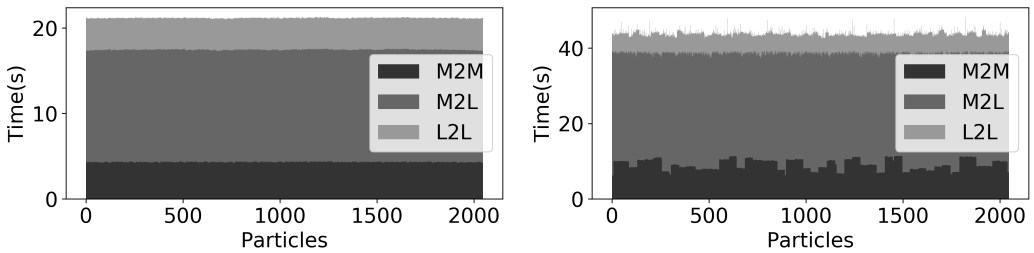


Fig. 6. Process execution times for a grid and a sphere geometry.

Next, we look at the performance for a sphere of diameter  $384\lambda$  discretized using 4,542,208 dipoles on the surface with a leaf box size of  $d_0 = 0.25\lambda$ , yielding an 11-level tree. This geometry is less balanced than the grid geometry (see the right subfigure of Fig. 7) as high level nodes can range from having no children due to no particles being in that part of the geometry at the leaf

$N_p$	Grid (s)				Speedup		Par Eff. (%)			
	M2M	M2L	L2L	Tot	Tot	M2M	M2L	L2L	Tot	
128	5.80	5.30	5.30	18.55	1.00	1.00	1.00	1.00	1.00	
256	3.06	4.13	2.66	11.21	1.65	0.95	0.64	0.99	0.83	
512	1.52	2.76	1.31	6.42	2.89	0.95	0.48	1.01	0.72	
1024	0.81	2.12	0.69	4.05	4.58	0.89	0.31	0.95	0.57	
2048	0.43	1.31	0.37	2.38	7.78	0.84	0.25	0.89	0.49	

Table 1. Performance of the MLFMA algorithm on the  $512\lambda$  grid geometry.

level, up to having a completely filled quad tree from the leaf level up to a high level node. This results in notable imbalance at the M2M level, which as discussed before, results in delays in the M2L execution. Note that there is an implicit barrier at the beginning of M2L processing, as an M2L interaction communication cannot proceed until both interacting processes have completed their M2M phases (though the faster process can perform local translations while waiting). Another (less significant) implicit barrier occurs at the beginning of L2L where nodes that are fully owned by a process must have all of the data from the translated parent node to perform antepolation on this parent node. The M2M execution range from the fastest to the slowest processes varies by as much as 84.5%. Despite this noticeable imbalance, the long execution times are not clustered among a small group of processes as one would see if each of the highest level tree nodes were to be handled by a single process without fine-grain parallelization. So even in this unbalanced geometry, the fine-grain parallel algorithm is helping to maintain a good load balance across process ranks.

## 5.2 Scalability

Next, we investigate the strong scaling efficiency of our parallel Helmholtz FMM algorithm, first on a surface and then on a volumetric structure.

For the 2D surface structure, we use the same  $512\lambda \times 512\lambda$  planar grid as above. As our base case for strong scaling efficiency, we use the performance on 128 cores because this is the smallest number of cores that this problem can be executed on due to its memory requirements. As seen in Table 1, both the interpolation and antepolation phases (M2M and L2L) perform very well with the increasing process counts, while M2L's performance falls off rapidly (down to 25% efficiency on 2048 cores). There are a couple of factors that contribute to this difference we observe in scaling characteristics. First factor is that M2M and L2L incur significant communications only at the highest level nodes, while M2L communications occur at every level where the source and observer nodes are on separate processes, which may essentially happen all the way down to the leaf nodes. Secondly, and more importantly, M2M and L2L computations involve relatively computation-heavy FFTs in between its communication steps. When the number of nodes in a level exceeds the number of processes, no process can own both a source and observer node of any translation, so all node data must be communicated. As the number of processes approaches the number of leaf nodes, the M2L communication bandwidth asymptotically approaches the worst case estimate. This means the increase in M2L bandwidth exceeds the worst case estimate increase as the number of processes approaches the number of leaf nodes. Despite M2L not scaling very well, the fine grained parallel algorithm presented still provides good speedups, nearly an 8x speedup when going from 128 to 2048 processes without showing any performance stagnation.

$N_p$	Volume (s)				Speedup		Par Eff. (%)			
	M2M	M2L	L2L	Tot	Tot	M2M	M2L	L2L	Tot	
128	0.527	2.15	0.526	3.26	1.00	1.00	1.00	1.00	1.00	
256	0.266	1.10	0.263	1.68	1.94	0.99	0.97	0.99	0.97	
512	0.14	0.679	0.135	0.99	3.27	0.93	0.79	0.97	0.82	
1024	0.079	0.380	0.084	0.574	5.68	0.83	0.71	0.78	0.71	
2048	0.051	0.271	0.058	0.406	8.03	0.65	0.50	0.57	0.50	

Table 2. Performance of the MLFMA algorithm on the  $32\lambda$  volumetric geometry.

$N_p$	Sphere (s)				Speedup		Par Eff. (%)			
	M2M	M2L	L2L	Tot	Tot	M2M	M2L	L2L	Tot	
128	6.71	13.54	5.29	26.76	1.00	1.00	1.00	1.00	1.00	
256	3.86	10.05	2.7	18.00	1.49	0.87	0.67	0.97	0.74	
512	2.34	6.20	1.46	11.04	2.42	0.72	0.55	0.91	0.61	
1024	1.23	4.32	0.72	7.70	3.47	0.68	0.39	0.92	0.43	
2048	0.92	3.19	0.416	5.58	4.79	0.46	0.26	0.79	0.30	

Table 3. Performance of the MLFMA algorithm on the  $384\lambda$  diameter sphere geometry.

Next, we examine strong scaling on a  $32\lambda \times 32\lambda \times 32\lambda$  volumetric structure (Table 2). From 128 to 512 processes, we observe very good scaling (80% overall efficiency), but then parallel efficiency drops off quickly (down to 50% overall at 2048 cores). In a volumetric problem, each tree node has a large number of nodes in its far-field (up to 189). Therefore the overall execution time is largely dominated by the M2L stage which does not manifest good scaling. The ideal scenario for our fine-grained parallel algorithm is when the nodes of a given level are distributed evenly among the processes, i.e., when the number of processes divides evenly into the number of nodes in a level or vice versa. This does not occur at 1024 or 2048 processes for this particular volumetric problem. Nevertheless, the overall speedup remains at around 8x when going from 128 to 2048 processes.

Finally, we look at scaling on the  $384\lambda$  sphere (Table 3). As seen in the load balance analysis of the previous subsection, load imbalances result in the faster processes having to wait for slower processes. This results in a noticeable drop in scaling efficiency of the M2M phase, where the imbalance has the greatest impact, as well as the M2L phase, where some processes that are already in their M2L phase have to wait for others that are still in their M2M phase. This also has an impact on the overall speedup. While increasing the number of processes continues to improve execution times, the speedup when going from 128 to 2048 processes is just under 5x in the sphere case.

### 5.3 Complexity Analysis

To help validate the complexity analysis presented in Sect. 4, the software was instrumented to report the computational cost, the number of messages sent and the size of these messages. In accordance with the geometries analyzed in Sect. 4, data was collected on the grid geometries

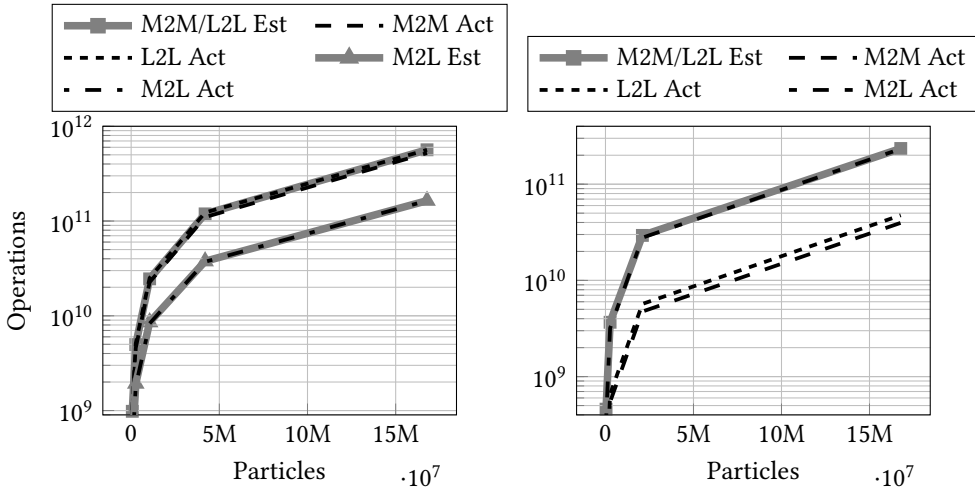


Fig. 7. Actual vs. estimated computational complexity. The left subfigure shows results for the surface geometry, while the right subfigure is for the volume geometry.

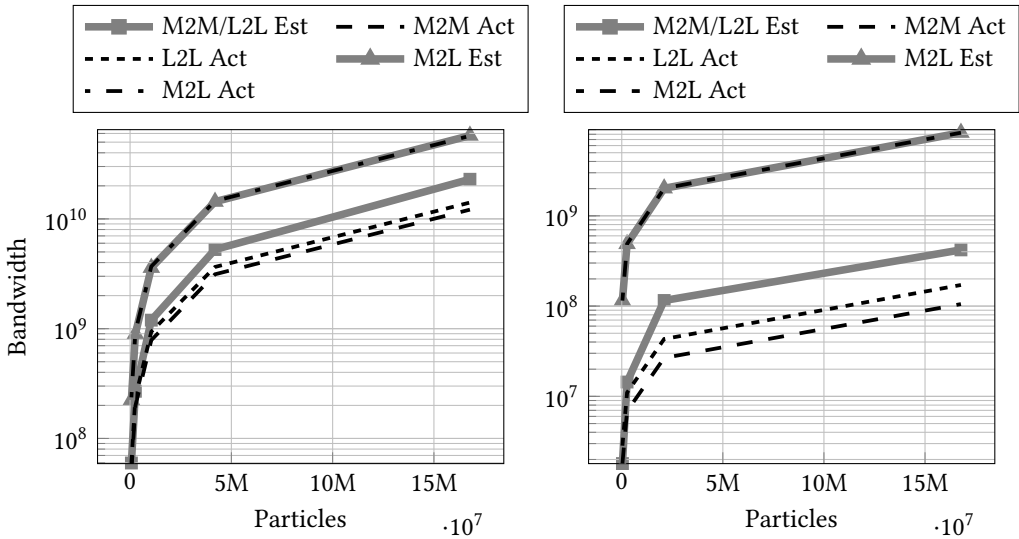


Fig. 8. Actual vs. estimated communication volume. The left subfigure shows results for the surface geometry, while the right subfigure is for the volume geometry.

ranging from  $64\lambda$  to  $1024\lambda$  and volume geometries ranging from  $16\lambda$  to  $16\lambda$  to as these geometries produce perfect quadtrees of heights ranging from 9 to 13 levels and octrees of heights ranging from 7 to 11 levels, respectively. As complexity estimates are asymptotic, they are scaled by least-squares fit to help visualize how well the estimates match the actual measurements.

Figure 7 shows the actual vs. the estimated overall computational complexities for the surface and volume geometries. The actual complexities match the estimates very closely. This indicates that the implementation of this algorithm does not have any unnecessary overhead costs in computation as computation is near to the ideal for Helmholtz FMM.

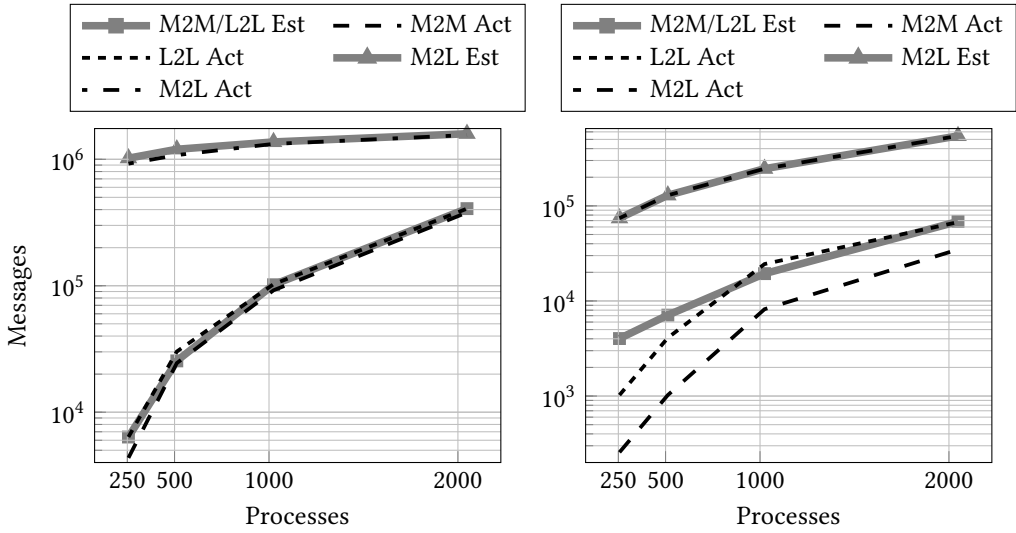


Fig. 9. Message counts vs expected Big-O message counts. The left diagram shows analysis of a surface geometry, while the right diagram shows analysis of a volume geometry.

Figure 8 shows the actual vs the estimated communication volumes for each phase separately. Of note is how the measured communication volume drops off relative to the estimate. We believe this is due to the number of samples producing a tree with more nodes at lower levels than the number of processes. Hence, many nodes are fully owned by a single process and require no communication during M2M or L2L. Increasing the number of processes would lead to more levels with plural nodes, bringing the communication volume closer to our estimates. M2L does not show the same communication volume falloff as M2M and L2L compared to the estimated volume because fully owned nodes still require data from the source nodes to be communicated to the process owning the observer node. Such communications will be required all the way down to the leaf nodes.

Figure 9 shows the measured worst case messages vs the estimated worst case messages for M2M and L2L. M2M and L2L Message counts are dominated by the  $P^2$  complexity of the all to all communications and the actual message count reflects this. The M2L prediction simplifies a very complex process that results in the number of M2L messages that are communicated.

#### 5.4 Process Alignment

In Table 4, we compare the number of packets sent between Rank Ordered and Process Aligned schemes during M2M and L2L phases for the  $512\lambda$  grid geometry. We observe a notable reduction in the number of messages exchanged, and hence the overall bandwidth, for lower process counts and continued reduction at higher process counts as expected. This reduction is likely to be effective in the relatively good scaling characteristics of M2M and L2L phases.

#### 5.5 Memory Utilization

Table 5 shows the memory utilization of the three data structures with largest memory needs with increasing process counts. As expected, the memory used for tree storage (Tree Mem) does not increase with process count, despite some fluctuations due to different partitionings of the leaf nodes. This shows that the tree data structure is being nicely partitioned across processes. Size of the translation operators (Trans Ops) increase slowly with process count, slightly more than doubling

$N_p$		128	256	512	1024	2048
<b>Rank Ordered</b>	M2M Bandwidth	1714	1872	3009	3126	4246
	L2L Bandwidth	1206	1166	2429	2382	3649
	Combined Bandwidth	2920	3038	5438	5508	7895
<b>Process Aligned</b>	M2M Bandwidth	1468	1662	2711	3272	4412
	L2L Bandwidth	960	955	2131	2104	3338
	Combined Bandwidth	2428	2617	4842	5376	7750
<b>Delta</b>		-492	-421	-596	-132	-145

Table 4. Comparison of the number of packets sent between Rank Ordered and Process Aligned schemes for the  $512\lambda$  grid geometry in millions of packets sent.

$N_p$	S/R Buffs	Trans Ops	Tree Mem
128	1.652	107.479	52.741
256	4.487	141.006	61.953
512	102.661	162.204	52.768
1024	256.982	199.047	62.028
2048	431.797	221.362	52.809

Table 5. Total memory utilization (in GBs) by the three largest data structures for the  $512\lambda$  grid geometry.

going from 128 to 2048 processes. This is due to the spatial distribution of the tree nodes; multiple source observer pairs with the same translation in the tree may belong to different processes. Particularly, as the process count increases and the number of nodes in a process decreases. This results in some processes storing some of the same translation operators as the other processes. The greatest memory increase is in the message buffers (S/R Buffs). The translation send and receive buffers (S/R Buffs) are used to communicate the data for source nodes that interact with nodes in another process. Single node communications for each source and observer pair would eliminate the need for this buffer, but would result in drastically more translation messages which would degrade performance. So the translation message buffers are maximized to use any remaining memory to limit the number of translation messages that must be sent.

On the other end of what can be performed with H-FMM is the volume geometry. Here the number of nodes per level is significantly increased due to the underlying full oct-tree structure (as opposed to a quad tree for a surface geometry), but the maximum height of a tree that can be computed is reduced. Most memory is reduced due to the shorter height of the tree, which reduces the size of the nodes at the top of the tree. However, the translation message buffers still use up as much memory as possible to improve translation communication performance.

## 5.6 Performance Comparison with Other Codes

Finally, we seek to compare our approach against those code that are available in the public domain. We note that open-source H-FMM codes are almost non-existent, with Abduljabbar et al. [1] being

$N_p$	S/R Buffs	Trans Ops	Tree Mem
128	3.110	6.559	5.012
256	8.402	10.095	5.161
512	22.264	16.301	5.457
1024	31.889	21.396	5.102
2048	51.736	30.390	5.414

Table 6. Total memory utilization (in GBs) by the three largest data structures for the  $32\lambda$  volume geometry.

a recent exception. Their BEMFMM code discretizes a mesh; the discretized points are used as particle inputs to our H-FMM code in order to compare processing of the same geometry. We ran a spherical geometry with 240 thousand mesh elements that produces 1.44 million points. Both codes are configured to produce a 6 level tree with slightly over 4100 leaf nodes with this sphere geometry and run with 64 nodes and 2048 MPI ranks. With this configuration, the BEMFMM implementation runs a single FMM iteration in 18.686 while our fine grain parallel FMM runs in 0.483 seconds. Our fine grain parallel Helmholtz FMM algorithm shows significantly faster performance in comparison.

## 6 CONCLUSIONS AND FUTURE WORK

We have demonstrated a novel method for parallel computation of large, upper level tree nodes in large-scale Helmholtz FMM which helps alleviate a key performance bottleneck associated with node dependency. The complexity of this method has been characterized. The results presented support the provided characterization and show the balance provided by this method.

Beyond the improvements presented, further work can be performed to improve memory usage. One possible method is a hybrid approach of MPI parallel with thread parallel to exploit shared memory parallelism to reduce duplicate memory allocation and communications.

## ACKNOWLEDGMENT

This research has in part been funded by the NSF Grant CCF-1822932. It has used computational resources at the National Energy Research Scientific Computing Center, a DOE Office of Science User Facility supported by the Office of Science of the U.S. Department of Energy under Contract No. DE-AC02-05CH11231, and at the High Performance Computing Center at Michigan State University.

## REFERENCES

- [1] Mustafa Abduljabbar, Mohammed Al Farhan, Noha Al-Harhi, Rui Chen, Rio Yokota, Hakan Bagci, and David Keyes. 2019. Extreme scale FMM-accelerated boundary integral equation solver for wave scattering. *SIAM Journal on Scientific Computing* 41, 3 (2019), C245–C268.
- [2] Emmanuel Agullo, Bérenger Bramas, Olivier Coulaud, Eric Darve, Matthias Messner, and Toru Takahashi. 2014. Task-based FMM for multicore architectures. *SIAM Journal on Scientific Computing* 36, 1 (2014), C66–C93.
- [3] A. Appel. 1985. An efficient program for many-body simulations. *SIAM J. Sci. Comput.* 6 (1985), 85–103.
- [4] J. Barnes and P. Hut. 1986. A hierarchical  $((n \log n)$  force calculation algorithm. *Nature* 324 (1986), 446–449.
- [5] Cris Cecka and Eric Darve. 2013. Fourier-based fast multipole method for the Helmholtz equation. *SIAM Journal on Scientific Computing* 35, 1 (2013), A79–A103.
- [6] W.C. Chew, E. Michielssen, J. M. Song, and J. M. Jin (Eds.). 2001. *Fast and Efficient Algorithms in Computational Electromagnetics*. Artech House, Inc., Norwood, MA, USA.
- [7] Weng Cho Chew, Eric Michielssen, JM Song, and Jian-Ming Jin. 2001. *Fast and efficient algorithms in computational electromagnetics*. Artech House, Inc.

- [8] B. Dembart and E. Yip. 1995. A 3D fast multipole method for electromagnetics with multiple levels. In *Proceedings of the 11th Annual Conference on Applied Computational Electromagnetics*, Vol. 1. Monterey, CA, 621–628.
- [9] B. Dembart and E. Yip. 1998. The accuracy of fast multipole methods for Maxwell's equations. *IEEE Computational Science and Engineering* 5 (1998), 48–56.
- [10] Ozgur Ergul. 2011. Parallel implementation of MLFMA for homogeneous objects with various material properties. *Progress In Electromagnetics Research* 121 (2011), 505–520.
- [11] Özgür Ergül. 2011. Solutions of large-scale electromagnetics problems involving dielectric objects with the parallel multilevel fast multipole algorithm. *JOSA A* 28, 11 (2011), 2261–2268.
- [12] Ö Ergül and L Gürel. 2008. Hierarchical parallelisation strategy for multilevel fast multipole algorithm in computational electromagnetics. *Electronics Letters* 44, 1 (2008), 3–5.
- [13] Ozgur Ergul and Levent Gürel. 2013. Accurate solutions of extremely large integral-equation problems in computational electromagnetics. *Proc. IEEE* 101, 2 (2013), 342–349.
- [14] Özgür Ergül and Levent Gürel. 2013. Fast and accurate analysis of large-scale composite structures with the parallel multilevel fast multipole algorithm. *JOSA A* 30, 3 (2013), 509–517.
- [15] L. Greengard. 1988. *The rapid evaluation of potential fields in particle systems*. MIT Press, Cambridge, MA.
- [16] L. Greengard, J. Huang, V. Rokhlin, and S. Wandzura. 1998. Accelerating fast multipole methods for the Helmholtz equation at low frequencies. *IEEE Computational Science and Engineering* 5 (1998), 32–38.
- [17] L. Greengard and V. Rokhlin. 1987. A fast algorithm for particle simulations. *J. Comput. Phys.* 20 (1987), 63–71.
- [18] Tsuyoshi Hamada, Tetsu Narumi, Rio Yokota, Kenji Yasuoka, Keigo Nitadori, and Makoto Taiji. 2009. 42 TFlops Hierarchical N-body Simulations on GPUs with Applications in Both Astrophysics and Turbulence. In *Proceedings of the Conference on High Performance Computing, Networking, Storage and Analysis (SC '09)*. ACM, New York, NY, USA, Article 62, 12 pages. <https://doi.org/10.1145/1654059.1654123>
- [19] S Hughey, HM Aktulga, V Melapudi, B Shanker, M Lu, and E Michielssen. 2018. Parallel Non-Uniform MLFMA for Multiscale Electromagnetic Simulation. In *2018 IEEE International Symposium on Antennas and Propagation & USNC/URSI National Radio Science Meeting*. IEEE, 1837–1838.
- [20] S. Hughey, H. M. Aktulga, M. Vikram, M. Lu, B. Shanker, and E. Michielssen. 2019. Parallel Wideband MLFMA for Analysis of Electrically Large, Nonuniform, Multiscale Structures. *IEEE Transactions on Antennas and Propagation* 67, 2 (Feb 2019), 1094–1107. <https://doi.org/10.1109/TAP.2018.2882621>
- [21] Tomoaki Ishiyama, Keigo Nitadori, and Junichiro Makino. 2012. 4.45 Pflops Astrophysical N-body Simulation on K Computer: The Gravitational Trillion-body Problem. In *Proceedings of the International Conference on High Performance Computing, Networking, Storage and Analysis (SC '12)*. IEEE Computer Society Press, Los Alamitos, CA, USA, Article 5, 10 pages. <http://dl.acm.org/citation.cfm?id=2388996.2389003>
- [22] Michael P Lingg, Stephen M Hughey, and Hasan Metin Aktulga. 2018. Optimization of the Spherical Harmonics Transform based Tree Traversals in the Helmholtz FMM Algorithm. In *Proceedings of the 47th International Conference on Parallel Processing*. 1–11.
- [23] Vikram Melapudi, Balasubramaniam Shanker, Sudip Seal, and Srinivas Aluru. 2011. A scalable parallel wideband MLFMA for efficient electromagnetic simulations on large scale clusters. *Antennas and Propagation, IEEE Transactions on* 59, 7 (2011), 2565–2577.
- [24] Bart Michiels, Jan Fostier, Ignace Bogaert, and Daniel De Zutter. 2013. Performing large full-wave simulations by means of a parallel MLFMA implementation. In *Antennas and Propagation Society International Symposium (APSURSI), 2013 IEEE*. IEEE, 1880–1881.
- [25] Bart Michiels, Jan Fostier, Ignace Bogaert, and Daniël De Zutter. 2013. Weak scalability analysis of the distributed-memory parallel MLFMA. *Antennas and Propagation, IEEE Transactions on* 61, 11 (2013), 5567–5574.
- [26] Bart Michiels, Jan Fostier, Ignace Bogaert, and Daniel De Zutter. 2015. Full-Wave Simulations of Electromagnetic Scattering Problems With Billions of Unknowns. *Antennas and Propagation, IEEE Transactions on* 63, 2 (2015), 796–799.
- [27] Bart Michiels, Jan Fostier, Ignace Bogaert, Piet Demeester, and Daniël De Zutter. 2011. Towards a scalable parallel MLFMA in three dimensions. In *Computational Electromagnetics International Workshop (CEM), 2011*. IEEE, 132–135.
- [28] Naoshi Nishimura. 2002. Fast multipole accelerated boundary integral equation methods. *Applied mechanics reviews* 55, 4 (2002), 299–324.
- [29] Abtin Rahimian, Ilya Lashuk, Shravan Veerapaneni, Aparna Chandramowlishwaran, Dhairya Malhotra, Logan Moon, Rahul Sampath, Aashay Shringarpure, Jeffrey Vetter, Richard Vuduc, Denis Zorin, and George Biros. 2010. Petascale Direct Numerical Simulation of Blood Flow on 200K Cores and Heterogeneous Architectures. In *Proceedings of the 2010 ACM/IEEE International Conference for High Performance Computing, Networking, Storage and Analysis (SC '10)*. IEEE Computer Society, Washington, DC, USA, 1–11. <https://doi.org/10.1109/SC.2010.42>
- [30] John K Salmon. 1991. *Parallel hierarchical N-body methods*. Ph.D. Dissertation. California Institute of Technology.
- [31] J. Sarvas. 2003. Performing Interpolation and Anterpolation by the Fast Fourier Transform in the 3D Multilevel Fast Multipole Algorithm. *SIAM J. Numer. Anal.* 41 (2003), 2180–2196.

- [32] B. Shanker and H. Huang. 2007. Accelerated Cartesian expansions - A fast method for computing of potentials of the form  $R^{-v}$  for all real  $v$ . *J. Comput. Phys.* 226 (2007), 732–753.
- [33] J. M. Song, C. C. Lu, and W. C. Chew. 1997. MLFMA for electromagnetic scattering by large complex objects. *IEEE Transactions on Antennas and Propagation* 45 (1997), 1488–1493.
- [34] Hari Sundar, Rahul S Sampath, and George Biros. 2008. Bottom-up construction and 2: 1 balance refinement of linear octrees in parallel. *SIAM Journal on Scientific Computing* 30, 5 (2008), 2675–2708.
- [35] Jose Manuel Taboada, Marta G Araujo, Fernando Obelleiro Basteiro, José Luis Rodríguez, and Luis Landesa. 2013. MLFMA-FFT parallel algorithm for the solution of extremely large problems in electromagnetics. *Proc. IEEE* 101, 2 (2013), 350–363.
- [36] S Velamparambil, Jiming Song, and Weng Cho Chew. 2000. On the parallelization of electrodynamic multilevel fast multipole method on distributed memory computers. In *Innovative Architecture for Future Generation High-Performance Processors and Systems, 1999. International Workshop. IEEE*, 3–11.
- [37] M. Vikram, C. Knowles, B. Shanker, and L.C. Kempel. 2011. An Ultra-Wideband FMM for Multi-scale Electromagnetic Simulations. *27th Annual Review of Progress in Applied Computational Electromagnetics* (2011).
- [38] M. Vikram and B. Shanker. 2009. An incomplete review of fast multipole methods from static to wideband as applied to problems in computational electromagnetics. *Applied Computational Electromagnetics Society Journal* 27 (2009), 79.
- [39] Caleb Waltz, Kubilay Sertel, Michael Carr, Brian C Usner, John L Volakis, and Others. 2007. Massively parallel fast multipole method solutions of large electromagnetic scattering problems. *Antennas and Propagation, IEEE Transactions on* 55, 6 (2007), 1810–1816.
- [40] Stephen Wandzuraz. 1993. The Fast Multipole Method for the Wave Equation: A Pedestrian Prescription. *IEEE Antennas and Propagation Magazine* 35, 3 (1993), 7–12.
- [41] M.S. Warren and J.K. Salmon. 1993. A parallel hashed oct-tree N-body algorithm. In *Proc. Supercomputing*. 1–12.
- [42] Ming-Lin Yang, Bi-Yi Wu, Hong-Wei Gao, and Xin-Qing Sheng. 2019. A Ternary Parallelization Approach of MLFMA for Solving Electromagnetic Scattering Problems with Over 10 Billion Unknowns. *IEEE Transactions on Antennas and Propagation* (2019).
- [43] Lexing Ying, George Biros, and Denis Zorin. 2004. A kernel-independent adaptive fast multipole algorithm in two and three dimensions. *J. Comput. Phys.* 196, 2 (2004), 591–626.
- [44] Lexing Ying and Denis Zorin. 2004. A simple manifold-based construction of surfaces of arbitrary smoothness. *ACM Transactions on Graphics* 23 (August 2004), 271–275. Issue 3. <https://doi.org/10.1145/1015706.1015714>